Charge and topography patterned lithium niobate provides physical cues to fluidically isolated cortical axons

D. Kilinc,[1,2,a)] A. Blasiak,[1,b)] M. A. Baghban,[3] N. C. Carville,[2,4] A. Al-Adli,[1] R. M. Al-Shammari,[2,4] J. H. Rice,[4] G. U. Lee,[1,2,c)] K. Gallo,[3,d)] and B. J. Rodriguez[2,4,e)]
[1]*School of Chemistry, University College Dublin, Belfield, Dublin 4, Ireland*
[2]*Conway Institute of Biomolecular and Biomedical Research, University College Dublin, Belfield, Dublin 4, Ireland*
[3]*Department of Applied Physics, KTH—Royal Institute of Technology, Stockholm 10691, Sweden*
[4]*School of Physics, University College Dublin, Belfield, Dublin 4, Ireland*

(Received 8 November 2016; accepted 19 January 2017; published online 31 January 2017)

In vitro devices that combine chemotactic and physical cues are needed for understanding how cells integrate different stimuli. We explored the suitability of lithium niobate ($LiNbO_3$), a transparent ferroelectric material that can be patterned with electrical charge domains and micro/nanotopography, as a neural substrate. On flat $LiNbO_3$ z-surfaces with periodically alternating charge domains, cortical axons are partially aligned with domain boundaries. On submicron-deep etched trenches, neurites are aligned with the edges of the topographical features. Finally, we bonded a bicompartmental microfluidic chip to $LiNbO_3$ surfaces patterned by etching, to create isolated axon microenvironments with predefined topographical cues. $LiNbO_3$ is shown to be an emerging neuron culture substrate with tunable electrical and topographical properties that can be integrated with microfluidic devices, suitable for studying axon growth and guidance mechanisms under combined topographical/chemical stimuli. *Published by AIP Publishing.*
[http://dx.doi.org/10.1063/1.4975304]

There is a growing interest in micro/nano technologies developed for neuroscience research, particularly to study axonal growth and guidance.[1] Among these, methods for generating micro/nano-topographical features received particular attention since axons tend to align with and accelerate on longitudinal structures, i.e., grooves, for certain combinations of groove width and depth.[2–4] In fact, recent *in vivo* evidence[5–7] led to the hypothesis that axially aligned micron-scale topography which incorporates submicron-scale features is required for the effective recovery of long (>20 mm) peripheral nerve defects.[8]

Topography with micron-scale feature sizes is typically created *via* standard photolithography on suitable masking layers, whose pattern is subsequently transferred to the substrate typically through an etching process.[9] Features with submicron sizes, on the other hand, require a deep-UV or an electron beam lithography.[10] 3D-patterned substrates can be used to culture neurons directly or serve as molds for casting durable or biodegradable polymers such as polydimethylsiloxane (PDMS)[2,11] or poly-lactic-co-glycolic acid,[12] respectively, which then serve as neuron substrates. 3D neuron culture substrates can also be decorated with nano-patterned features, such as grooved fibers[13] and Ti nanotube arrays.[14]

Axonal growth cones not only sense the mechanical properties of their microenvironment but also actively generate force by pulling on focal adhesions such that local topography affects guidance decisions.[1] For example, combining topographical (e.g., 1 μm-wide and 400 nm-deep grooves) and biochemical (nerve growth factor) cues synergistically enhanced hippocampal axon length.[2] Therefore, experimental models that provide independent topographical and biochemical cues offer additional insight on neural growth and guidance mechanisms. Microfluidic devices that fluidically isolate axons from their cell bodies or provide exclusive access to specific subcellular regions are now commonly used in neurobiology.[15] Additionally, microfluidic devices are used to form gradients of chemotactic cues.[16] *In vivo*, growth cones may be remotely distant from their cell bodies and typically perceive guidance cues as chemical gradients. Thus, microfluidic chips help create physiologically-relevant *in vitro* model systems. However, micro/nano-topographical cues are rarely integrated into microfluidic devices.[17,18]

Lithium niobate ($LiNbO_3$) is a transparent ferroelectric material that has a spontaneous polarization, $P_S = 0.71\ \mathrm{C\ m^{-2}}$ along its z-axis, and is thus characterized by positive and negative bound polarization charges at the $+z$ and $-z$ crystal surfaces, respectively. Periodically poled $LiNbO_3$ (PPLN) contains periodic ferroelectric domains (alternating in $\pm z$), which are suitable for nonlinear optical applications. These domains can also be converted into topographical features due to their inherently different etch rates. Alternatively, topographical features can be created in monodomain substrates *via* photo- or electron beam lithography. Recent work showed that uncoated $LiNbO_3$ surfaces are biocompatible with cell-type specific effects: osteoblasts[19] and mesenchymal stem cells[20] exhibited increased proliferation and differentiation on charged $LiNbO_3$. For stem cells—but not for osteoblasts—positively charged $LiNbO_3$ was much more effective than negatively charged $LiNbO_3$. In fibroblasts, $LiNbO_3$ surface

[a)]Electronic mail: devrim.kilinc@pasteur-lille.fr. Current address: INSERM U1167, Institut Pasteur de Lille, Lille 59019, France.
[b)]Current address: Singapore Institute for Neurotechnology, Singapore 117456.
[c)]Electronic mail: gil.lee@ucd.ie
[d)]Electronic mail: gallo@kth.se
[e)]Electronic mail: brian.rodriguez@ucd.ie

charge was also shown to affect cell morphology and motility.[21] $LiNbO_3$ has recently been shown to be suitable for manipulating and sorting biological material. Exploiting the bulk photovoltaic effect, electric field patterns can be induced by illuminating $LiNbO_3$, which can be used to pattern spores and pollen.[22] Exploiting its pyroelectric properties, PPLN can also be used for generating permanent charge patterns on polymer membranes, which can then be used for cell patterning.[23] Furthermore, photorefractive properties of iron-doped $LiNbO_3$ can be used for electrode-free immobilization of bacteria *via* light-induced dielectrophoresis.[24] Finally, cell sorting can be achieved *via* acoustic waves by bonding $LiNbO_3$ to microfluidic devices.[25]

Here, we investigate the potential of $LiNbO_3$ as a neuron substrate, providing charge and topography patterns to fluidically isolated axons, where the combined effects of chemotactic, charge, and topography cues can be studied in controlled microfluidic environments. We show that neurites align with boundaries of charge and topography patterns, and that these patterns can be embedded in the axon microenvironment, towards a better understanding of axon growth behavior.

Primary embryonic mouse cortical neurons were harvested as previously described.[26] The culture medium consisted of DMEM-Glutamax supplemented with 10% fetal bovine serum, 1% Penicillin/Streptomycin solution (P/S), and B_{27} neuron supplement (all from Gibco). At 3 days *in vitro* (DIV), the culture medium was replaced with Neurobasal (Gibco) supplemented with 1% P/S and B_{27}. We first cultured neurons at 2×10^4 cells·cm^{-2} on z-plane-parallel cut congruent $LiNbO_3$ wafers (CasTech, Fuzhou, China) with uniform charge and on periodically poled, *z*-cut $LiNbO_3$ (Gooch & Housego, Palo Alto, CA) with a charge pattern with $\sim 30\,\mu$m domain period. Prior to characterization and cell culture, substrates were cleaned by consecutive rinsing with acetone, isopropanol, and de-ionized (DI) water. Atomic and piezoresponse force microscopy (AFM/PFM) were performed to probe surface topography and charge, respectively. For AFM, MFP-3D (Asylum Research, Santa Barbara, CA) was operated in the amplitude modulation mode with cantilevers having a typical resonant frequency of $\sim$330 kHz and a spring constant of $\sim$42 N m^{-1} (PPP-NCH; Nanosensors, Neuchatel, Switzerland). For PFM, DPE-XSC11 D (MikroMasch, Wetzlar, Germany) cantilevers having a typical force constant of 42 N m^{-1} and a resonant frequency of 350 kHz were used. PFM amplitude images show the sample deformation under the applied AC voltage as measured by the tip displacement and the corresponding cantilever deflection. PFM phase images show the phase lag of the tip oscillation with respect to the modulation voltage and indicate the direction of ferroelectric polarization and thereby the sign of the corresponding polarization charge at the surface.[27]

Neurons did not grow unless the substrates were coated with 2.5 μg/ml poly-L-lysine (PLL; Sigma, Wicklow, Ireland) in Dulbecco's phosphate buffered saline (DPBS; Lonza, Basel, Switzerland) overnight and rinsed 3× with DPBS. Cells were aldehyde-fixed on 3–6 DIV, stained to reveal β3-tubulin, F-actin, and nuclei, and mounted on microscope slides as previously described.[26] Neurite length was quantified

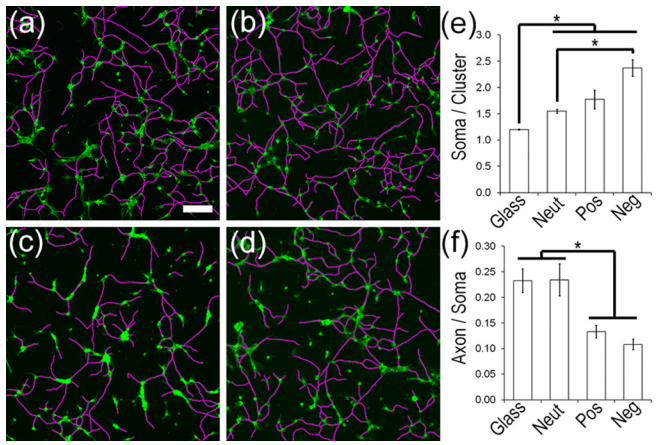

FIG. 1. Neural growth at 4 DIV on PLL-coated (a) glass and $LiNbO_3$ with uniform (b) neutral (*x*-cut), (c) negative (-*z*-cut), and (d) positive (+*z*-cut) charges. β3-tubulin immunostaining (green) was used to analyze morphometry. Software-generated neurite traces (purple) are shown as overlays. Scale bar = 100 μm. (e) and (f) Number of cell bodies per cell body cluster (Soma/Cluster) and number of axons longer than 60 μm per cell body (Axon/Soma) were quantified for all groups (N = 350 neurites on 3 samples). Error bars = standard error of the mean. One-way analysis of variance followed by *t*-test (*$p < 0.05$).

from tubulin staining using the NeuronJ plug-in[28] in ImageJ (NIH, Bethesda, MD). Cell clustering was quantified by dividing the number of clusters to the number of nuclei. A neurite length cut-off of 60 μm (1.5× median neurite length of control neurons grown on PLL-coated glass coverslips) was used before calculating the axon/soma ratio. Substrates were recovered and reused following imaging by carefully removing them from microscope slides and sonicating first in 2% PCC-54 detergent (Thermo-Fisher Scientific, Waltham, MA) in DI water, subsequently in DI water, and finally in isopropanol (20 min each). As shown in Figure 1, neurons exhibited increased clustering and decreased axonal connectivity on substrates with uniform charge, suggesting sub-optimal PLL coverages. Interestingly, the direction of the charge (i.e., negative or positive) did not affect the outcome, similar to the effects of charged $LiNbO_3$ on osteoblast proliferation and mineral accumulation.[19] Figure 2 shows neurons cultured on charge-patterned PPLN substrates. On these substrates, axons appeared to recognize and align with domain boundaries, reminiscent of the avoidance of domain boundaries by fibroblasts on a periodically poled lithium tantalate (PPLT).[29] To check if there was a preferential deposition of the positively charged PLL to negatively charged domains, we coated the substrate with fluorescein isothiocyanate-conjugated PLL (FITC-PLL; Sigma); however, no preferential deposition was detected (Fig. 2(a), inset). In future work, it will be important to elucidate the role of surface cleaning and functionalization in addition to the surface charge on the attachment and proliferation of different cell types.

We next cultured neurons on microtopographical features created *via* reactive ion etching on *y*-cut $LiNbO_3$. Etched samples were prepared from 500 μm-thick *y*-cut substrates (CasTech). A 160 nm Cr layer was deposited on the samples using an E-beam sputtering system (Auto 306 HV; Edwards, Crawley, UK), which acted as a hard mask. Spin-coated Microposit S1813 photoresist (Shipley, Marlborough, MA) was patterned via a photomask (Photronics, Brookfield,

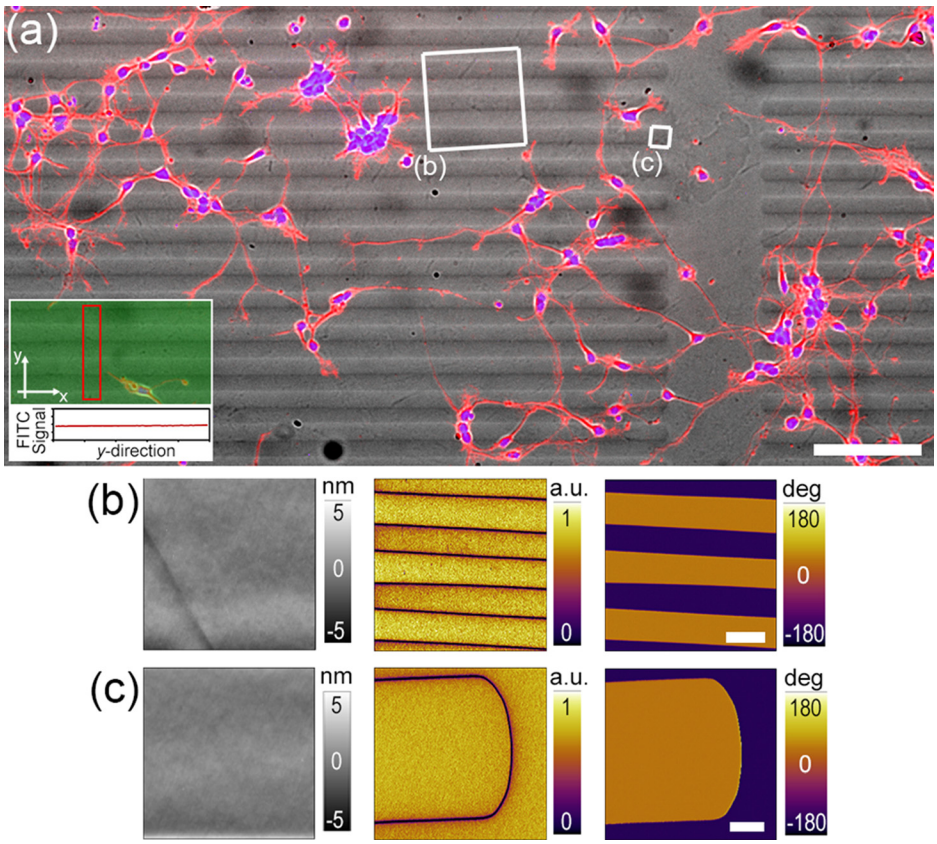

FIG. 2. Neural growth on a flat PPLN with periodically alternating charge patterns. (a) Overlay of phase contrast image of the charge domains with F-actin (red) and nuclear (blue) staining. Inset shows the FITC-PLL staining (green overlay) and the average fluorescence intensity in the red rectangle along the *y*-axis. (b) and (c) AFM topography, PFM amplitude, and PFM phase maps of representative regions marked in (a). Scale bars = 100 μm (a); 20 μm (b); and 4 μm (c).

CT), and developed using Microposit MF319 (Shipley). An Inductively Coupled Plasma-Reactive Ion Etching machine (ICP RIE; Plasmalab 100; Oxford Instruments, Abingdon, UK) was used to transfer the pattern first to the Cr mask and then to the $LiNbO_3$ sample using Cl_2/O_2 and SF_6/Ar plasma combinations, respectively. The RIE etch time was adjusted to achieve 550 nm-deep features. The etched patterns consisted of 1D parallel microgrooves with 40 μm-spacing and widths varying from 2 to 10 μm, and 2D 10 μm-wide hexagonal pits in a hexagonal array with a period of 31 μm.

Axon alignment to microgrooves was quantified from the F-actin staining images using ImageJ. Multi-step image processing was conducted to exclude the cell body signals. Using the processed image, F-actin staining intensities were measured on the edges of grooves—a pair of 1.3 μm-wide stripes for each groove—and compared with identical stripes immediately adjacent to the groove edges (outside grooves). Two major observations were made: (1) axons typically elongated parallel to the microgrooves, preferentially aligning with their edges, as evidenced by approximately 1.2× higher neurite staining on groove edges relative to other areas (Fig. 3); (2) fine neurites appeared to follow hexagonal pits (Fig. 4). These observations are consistent with the literature, where the tendency of neurites to elongate along edges[9,11] and channels[1] has been repeatedly demonstrated. Groove or ridge width appears to be the main factor determining the alignment of neurites to topographical features, where 200 nm and 500–1000 nm widths have been shown to be ideal for dorsal root ganglia neurons[4] and differentiating PC12 cells,[3] respectively.

Finally, to test microfluidic integration with microtopography, we bonded a bicompartmental neuron culture device to etched $LiNbO_3$ substrates *via* oxygen plasma-mediated surface activation (PE-100 plasma system; PlasmaEtch, Carson City, NV). Fabrication of PDMS (Sylgard 184; Dow Corning, Midland, MI) microfluidic devices was previously

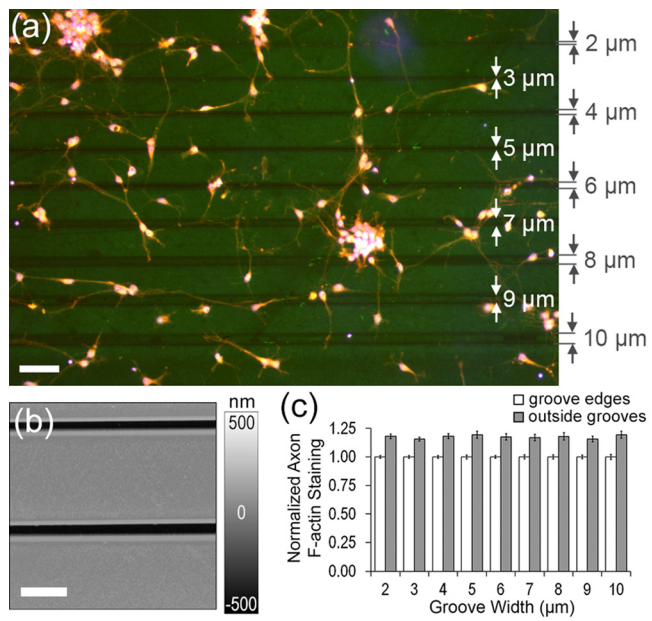

FIG. 3. Neurites align with the edges of 550 nm deep features. (a) F-actin (red) and nuclear staining (blue) of cortical neurons cultured on a $LiNbO_3$ substrate with 2–10 μm wide parallel grooves, coated with FITC-PLL (green). (b) AFM image of the groove pattern. (c) Mean neurite F-actin staining intensity on groove edges (gray), normalized by the staining intensity in adjacent areas outside grooves (white) as a function of groove width. Error bars = SEM. For all groove widths, neurite staining was significantly higher on groove edges compared to adjacent areas ($p < 10^{-4}$; paired *t*-test). Scale bars = 50 μm (a) and 20 μm (b).

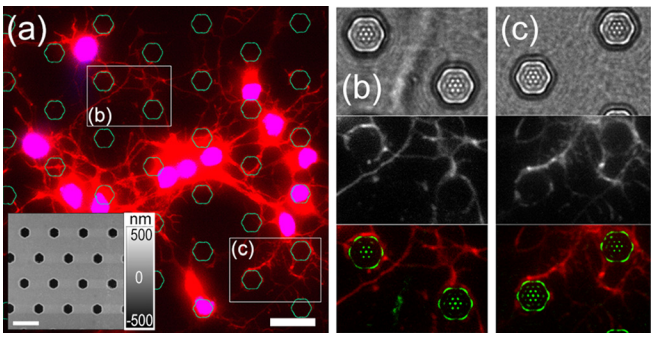

FIG. 4. Neurites align with the edges of 550 nm deep features. (a) Neurons, cultured on the $LiNbO_3$ substrate with hexagonal pits, stained for F-actin (red) and nuclei (blue). Inset shows the AFM image of the substrate. (b) and (c) Marked areas in (a) are 2.5× magnified to show fine neurites aligning with the edges of the pits. The contours in the bright field image (green) were superimposed on the F-actin staining (red). Scale bars = 20 μm.

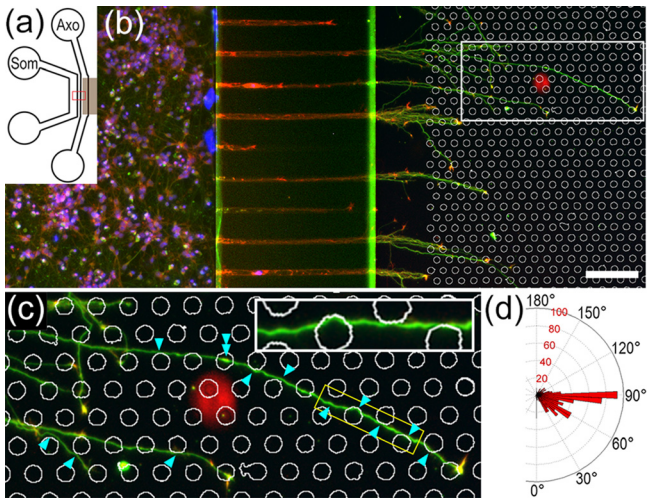

FIG. 5. Fluidic isolation of cortical axons on the etched $LiNbO_3$ substrate. (a) Layout of the bicompartmental microfluidic chip consisting of the somatic (Som) and axonal (Axo) chambers, connected *via* parallel microchannels (not drawn). The brown area indicates the location of the aligned etch pattern. (b) Microfluidic neuron culture on the etched *y*-cut $LiNbO_3$ substrate (red boxed area in (a)), showing β3-tubulin (green), F-actin (red), and nuclei (blue), superposed with the etch pattern (white). Scale bar = 100 μm. (c) Marked area in (b) is 2.6× magnified to show the deformations in axon shafts. Axons follow the edges of microstructures (arrowheads). Occasionally, when an axon shaft crosses through a pit, increased cytoskeletal density was observed (double arrowhead). Inset: the axon segment in the yellow box is 2× magnified. (d) Angular histogram of axon segments on the entire patterned region in the axonal chamber (numbers of axon segments given in red). Axon segments are typically aligned at 0° or 30° with respect to the microchannels (90° in the histogram) as they navigate through the hexagonal pits pattern.

described.[30] The devices consist of two compartments—somatic and axonal—interconnected by parallel microchannels that permit axonal growth. The "hexagonal pits" pattern was manually aligned with the axonal compartment during bonding such that axons emanating from the microchannels encountered an array of pits. Bonded devices were filled with DI water and sterilized with a 30 min exposure to UV light. Both compartments were incubated with 10 μg ml^{-1} PLL in DPBS overnight at 37 °C and rinsed with DPBS prior to cell seeding. Neurons were seeded in the somatic chamber with a seeding density of approximately 8×10^5 cells·cm^{-2}. Cells were allowed to attach for 5 min, and subsequently, all wells were filled with the culture medium. Devices were placed in Petri dishes and 1 ml of 0.1% ethylenediaminetetraacetic acid (EDTA; Sigma) in DI water was added to the side of the dish to minimize evaporation during incubation (37 °C, 5% CO_2). Immunocytochemistry in these devices followed the same protocol with minor adaptations as described previously.[30] Substrates that were bonded to microfluidic chips were also recovered and reused. Substrates were first sonicated in detergent solution for 30 min, and the chips were carefully removed by pushing from edges. Following separation, substrates were cleaned using the same protocol as for non-bonded substrates. Any remnant PDMS was scraped off using a scalpel, and the cleaning procedure was repeated. Topographical features did not interfere with device bonding or fluidic isolation, and axons appeared to avoid the pits (Fig. 5). Analysis of axon paths suggested that most axonal segments were parallel to or made 30° angles with the direction of microchannels, suggesting that the axons navigated through the hexagonal pits pattern by forming point contacts with the edges of the pits and avoiding the 3D topography.

Overall, this work demonstrates the culture of neurons on uniform $LiNbO_3$, etched $LiNbO_3$, and PPLN, and expands on previous studies on the growth of other cell types on uniform $LiNbO_3$ (Ref. 19) and PPLT.[29] The results point to promising research directions exploiting $LiNbO_3$ as a neural substrate. Potentially, these can be combined with further control and sensing capabilities afforded by the photonic and piezoelectric properties of this material, already widely used for the nonlinear optical frequency-conversion of conventional lasers and to generate standing[31] and traveling[32] surface acoustic waves for sorting particles or cells in flow channels. Moreover, the topography patterning and microfluidic integration capabilities demonstrated with this work indicate $LiNbO_3$ as a promising material template for developing highly complex *in vitro* neuron culture devices, which allow controlling not only the surface topography but also the local chemical microenvironment.

In summary, $LiNbO_3$ is an emerging neuron culture substrate with optical, electrical, and topographical properties that can be engineered to design complex experimental model systems, potentially capable of stimulating and sensing neurons at the subcellular level in a topographically and chemically defined microenvironment.

This work was supported by the Nanoremedies Programme funded under the Programme for Research in Third-Level Institutions of Higher Education Authority and co-funded under the European Regional Development Fund, by the UCD Research (SF1253), and by the Swedish Research Council (VR 622-2010-526 and 621-2014-5407). The AFM used for this work was funded by Science Foundation Ireland (07/IN1/B931).

[1]D. Kilinc, A. Blasiak, and G. U. Lee, Front. Cell. Neurosci. **9**, 282 (2015).
[2]N. Gomez, Y. Lu, S. Chen, and C. E. Schmidt, Biomaterials **28**(2), 271 (2007).

[3]A. Ferrari, M. Cecchini, A. Dhawan, S. Micera, I. Tonazzini, R. Stabile, D. Pisignano, and F. Beltram, Nano Lett. **11**(2), 505 (2011).
[4]F. Johansson, P. Carlberg, N. Danielsen, L. Montelius, and M. Kanje, Biomaterials **27**(8), 1251 (2006).
[5]S. H. Hsu and H. C. Ni, Tissue Eng. Part A **15**(6), 1381 (2009).
[6]A. Hurtado, J. M. Cregg, H. B. Wang, D. F. Wendell, M. Oudega, R. J. Gilbert, and J. W. McDonald, Biomaterials **32**(26), 6068 (2011).
[7]H. Okamoto, K. Hata, H. Kagami, K. Okada, Y. Ito, Y. Narita, H. Hirata, I. Sekiya, T. Otsuka, and M. Ueda, J. Biomed. Mater. Res. **92A**(3), 859 (2010).
[8]E. C. Spivey, Z. Z. Khaing, J. B. Shear, and C. E. Schmidt, Biomaterials **33**(17), 4264 (2012).
[9]H. Francisco, B. B. Yellen, D. S. Halverson, G. Friedman, and G. Gallo, Biomaterials **28**(23), 3398 (2007).
[10]A. Rajnicek, S. Britland, and C. McCaig, J. Cell Sci. **110**(23), 2905 (1997).
[11]N. Li and A. Folch, Exp. Cell. Res. **311**(2), 307 (2005).
[12]C. Miller, S. Jeftinija, and S. Mallapragada, Tissue Eng. **8**(3), 367 (2002).
[13]E. Kang, G. S. Jeong, Y. Y. Choi, K. H. Lee, A. Khademhosseini, and S. H. Lee, Nat. Mater. **10**(11), 877 (2011).
[14]J. A. Sorkin, S. Hughes, P. Soares, and K. C. Popat, Mater. Sci. Eng. C Mater. Biol. Appl. **49**, 735 (2015).
[15]A. D. Jadhav, L. Wei, and P. Shi, Curr. Neuropharmacol. **14**(1), 72 (2016).
[16]A. M. Taylor, S. Menon, and S. L. Gupton, Lab Chip **15**(13), 2781 (2015).
[17]Y. Yang, K. Kulangara, J. Sia, L. Wang, and K. W. Leong, Lab Chip **11**(9), 1638 (2011).
[18]A. Kundu, L. Micholt, S. Friedrich, D. R. Rand, C. Bartic, D. Braeken, and A. Levchenko, Lab Chip **13**(15), 3070 (2013).
[19]N. C. Carville, L. Collins, M. Manzo, K. Gallo, B. I. Lukasz, K. K. McKayed, J. C. Simpson, and B. J. Rodriguez, J. Biomed. Mater. Res. A **103**(8), 2540 (2015).
[20]J. Li, X. Mou, J. Qiu, S. Wang, D. Wang, D. Sun, W. Guo, D. Li, A. Kumar, X. Yang, A. Li, and H. Liu, Adv. Healthcare Mater. **4**(7), 998 (2015).
[21]V. Marchesano, O. Gennari, L. Mecozzi, S. Grilli, and P. Ferraro, ACS Appl. Mater. Interfaces **7**(32), 18113 (2015).
[22]M. Jubera, I. Elvira, A. García-Cabañes, J. L. Bella, and M. Carrascosa, Appl. Phys. Lett. **108**(2), 023703 (2016).
[23]R. Rega, O. Gennari, L. Mecozzi, S. Grilli, V. Pagliarulo, and P. Ferraro, Adv. Mater. **28**(3), 454 (2016).
[24]L. Miccio, V. Marchesano, M. Mugnano, S. Grilli, and P. Ferraro, Opt. Laser Eng. **76**, 34 (2016).
[25]D. J. Collins, A. Neild, and Y. Ai, Lab Chip **16**(3), 471 (2016).
[26]A. Blasiak, G. U. Lee, and D. Kilinc, ACS Chem. Neurosci. **6**(9), 1578 (2015).
[27]D. Denning, J. Guyonnet, and B. J. Rodriguez, Int. Mater. Rev. **61**(1), 46 (2016).
[28]E. Meijering, M. Jacob, J. C. F. Sarria, P. Steiner, H. Hirling, and M. Unser, Cytometry Part A **58**(2), 167 (2004).
[29]C. Christophis, E. A. Cavalcanti-Adam, M. Hanke, K. Kitamura, A. Gruverman, M. Grunze, P. A. Dowben, and A. Rosenhahn, Biointerphases **8**(1), 27 (2013).
[30]D. Kilinc, A. Blasiak, J. J. O'Mahony, and G. U. Lee, Sci. Rep. **4**, 7128 (2014).
[31]O. Jakobsson, C. Grenvall, M. Nordin, M. Evander, and T. Laurell, Lab Chip **14**(11), 1943 (2014).
[32]L. Schmid, D. A. Weitz, and T. Franke, Lab Chip **14**(19), 3710 (2014).